Reciprocating compressor valve condition monitoring using image-based pattern recognition

John N. Trout[1] and Jason R. Kolodziej[2]

[1,2] *Department of Mechanical Engineering, Rochester Institute of Technology, Rochester, New York, 14623, USA*
jxt6193@rit.edu
jrkeme@rit.edu

ABSTRACT

This work presents the development of a vibration-based condition monitoring method for early detection and classification of valve wear within industrial reciprocating compressors through the combined use of time-frequency analysis with image-based pattern recognition techniques. A common valve related fault condition is valve seat wear that is caused by repeated impact and accentuated by chatter. Seeded faults consistent with valve seat wear are introduced on the crank-side discharge valves of a Dresser-Rand ESH-1 industrial compressor. A variety of operational data including vibration, cylinder pressure, and crank shaft position are collected and processed using a time-frequency domain approach. The resulting diagrams are processed as images with features extracted using 1st and 2nd order image statistics. A Bayesian classification strategy is employed with accuracy rates greater than 90% achieved using two and three-dimensional features spaces.

1. INTRODUCTION

Modern reciprocating compressors are the culmination of over 100 years of design and manufacturing experience and are one of the most widely employed compressor technologies in today's industry. They operate reliably at a wide range of pressures, can compress a large variety of gas, and are highly adaptable thanks to multi-stage capabilities. However, reciprocating compressors suffer from relatively high maintenance costs — sometimes costing more than three times to maintain than centrifugal compressors. The majority of reciprocating compressor downtime and maintenance costs can be attributed to the compressor valves, which account for 36% of shut downs and 50% of total repair costs (Schirmer, Fernandes, & Caux, 2004). Continuous condition monitoring of valves and related components can provide significant reduction in overall maintenance costs and provide a basis for preventative maintenance programs.

The most common approach employed for condition monitoring in reciprocating compressors is through the use of the pressure-volume (P-V) curve. This is a well understood method that utilizes the geometry and motion of the compressor to determine theoretically the compressor's performance. When measurement of the P-V diagram deviates from the predicted certain failure modes are likely. While this method has proven successful it does require the use of real-time measurement of in-cylinder pressure which adds expense and additional maintenance. Another typical monitoring method is through vibration analysis, which look for changes in a machines typical vibration signature due to a fault condition. The vibration for reciprocating machines are characterized by a series of periodic events such as combustion, piston slap, valve opening and closing, etc, all which produce a highly cyclic vibration signature (Randall, n.d.). This type of vibration signal is described as cyclostationary, which is a non-stationary signal whose statistical properties change periodically, or cyclically, with time. All cyclostationary signals exhibit some periodicity in their energy profile, giving rise to key characteristics which are used to identify statistically significant variation due to changes in operating condition (Antoni, 2009). Due to the cyclostationary nature of the measurement, time-frequency transforms are used which retain time and frequency domain behavior of a given signal, revealing its non-stationary and periodic nature common in reciprocating compressors. A portion of this research is based on the concept of compressor's cyclostationary motion and time-frequency analysis.

A variety of research has been done investigating valve fault detection in reciprocating compressors. Liang et. al. developed a procedure to detect valve faults using the smoothed-pseudo Wigner-Ville Distribution which revealed characteristic patterns due to impact response vibration (Liang, Gu, Ball, & Henry, 1996). Elhaj et. al. investigated early detection of valve leakage through the extraction of detection

features using Continuous Wavelet Transforms of both vibration and acoustic measurements (Elhaj, Gu, Ball, Shi, & Wright, 2001). They later combined the monitoring of instantaneous angular speed (IAS) and dynamic cylinder pressure to develop a reliable means of detecting valve leakage (Elhaj, Almrabet, Rgeai, & Ehtiwesh, 2010). Antoni et. al. has completed much work on the use of cyclo-stationary modeling for the purposes of reciprocating machine condition monitoring. In regards to valve faults, he developed a means for identifying simple fault indicators through the use of the Wigner-Ville Spectrum (Zouari et al., 2007)(Antoni, 2009). Lin et. al. examined the use of time-frequency analysis for reciprocating compressor vibration signals with a neural network for automated condition classification (Yih-Hwang, Liu, & Wu, 2006) and later applied this to valve fault classification using seeded faults (Yih-Hwang, Liu, & Wu, 2009). In 2013, using the compressor in this work, Guerra et. al. developed a mechanical-thermodynamic model of the compressor and investigated health monitoring of discharge valves using P-V diagrams, dynamic pressure measurements, and frequency domain analysis (Guerra & Kolodziej, 2014). Later, Holzenkamp et. al. included modeling and simulation of the main journal bearing as well condition monitoring of common main bearing faults (Holzenkamp, Kolodziej, Boedo, & Delmotte, 2016).

The current work advances previous health monitoring research completed by Guerra et. al. by incorporating time-frequency analysis of vibration measurements into the detection of valve related faults. Using time-frequency analysis combined with image-based feature extraction an effective vibration-based method for early detection of valve wear within industrial reciprocating compressors is developed. One of the more common valve related fault conditions is valve seat wear and is investigated at various degrees of severity on the crank-side discharge valves of Dresser-Rand ESH-1 compressor (Fig. 1). Using a variety of operational data including vibration, cylinder pressure, and crank shaft position, a condition monitoring method is developed to detect the severity of the particular fault. Nominal (healthy) and fault condition (non-healthy) valves are seeded in the compressor and operating data analyzed using the Short-time Fourier Transform. The resulting time-frequency diagrams are processed as images and fault detection features are extracted using texture statistics. A Bayes classifier is trained to identify fault severity and verified through use of validation data. The effectiveness of each time-frequency method to reveal fault signatures is evaluated based on classifier performance.

2. TIME-FREQUENCY ANALYSIS

Traditional spectral analysis techniques, such the Fourier transform, estimate the frequency content of a signal or function over its entire length. Such methods are ideal for analyzing stationary, or non-time varying, signals. However, when considering non-stationary signals, such as those produced by reciprocating machines, it is often valuable to know how the frequency spectrum of a signal varies with respect to time. Numerous time-frequency analysis techniques have been developed to provide both time and frequency information of a given signal such as the Short-Time Fourier Transform (STFT), the Wigner-Ville Distribution and Continuous Wavelet Transform. For this exploratory research the STFT is employed because of its computation ease and its well established acceptance. The following section provides a brief overview of the STFT.

An STFT is performed by dividing a signal into short time segments and applying the Fourier transform to each segment. The resulting spectrum segments are combined to show how the spectrum of the signal varied with each time step. The STFT is given in discrete form by,

$$STFT(\tau, f_i) = \sum_{k=-\infty}^{\infty} x(k)w(k-\tau)e^{(\frac{-j2\pi k f_i}{N})} \quad (1)$$

where $w(k-\tau)$ is a short time window and $STFT(\tau, f_i)$ is a complex-valued function representing the frequency spectrum and is a function of both frequency and time. The chosen size of $w(k-\tau)$ effects the time and frequency resolution due to the uncertainty principle. The window shape provides

Figure 1. Dresser-Rand ESH-1 Compressor at RIT Compressor Test Cell

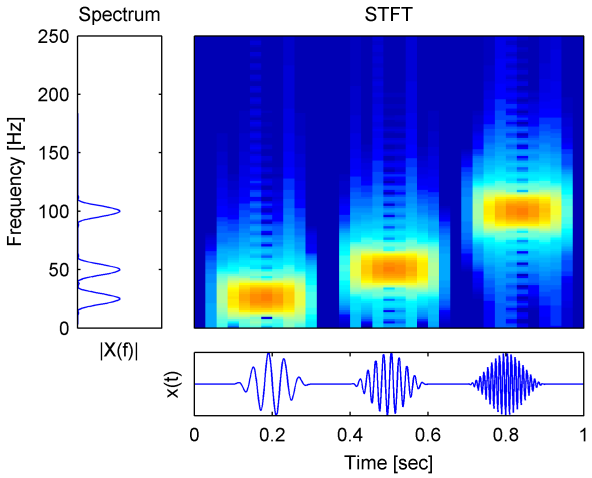

Figure 2. Short-time Fourier transform of non-stationary signal

a "smoothing" effect to the STFT while window overlapping is an option for signals with fast time-varying frequency content to reduce the loss of information at window edges. In general, the magnitude scale (linear vs log), window size, window shape, and overlap chosen will all effect the visual properties of the STFT and can be selected based on the given application or signal.

The STFT of an example signal is provided in Fig. (2). It is referred to in this work, generically, as a *time-frequency diagram* (TFD) and provides a visual representation of the time-frequency behavior of a signal. While there are other time-frequency analysis tools available the STFT is utilized in this work for its ease of implementation and proven success. The simulated example in the figure resembles the valve impact measured by the accelerometer during valve opening events. (Note: if a FFT was determined from the data the left plot in the figure results and tells nothing of the temporal component to the frequency spectrum)

3. COMPRESSOR TEST CELL AT RIT

The experimental test cell used in for this work is a Dresser-Rand ESH-1 reciprocating compressor located at the Rochester Institute of Technology's (RIT) Compressor Test Cell shown in Fig. 1. The single stage, dual acting compressor was donated by the Dresser-Rand and installed at RIT in 2010. One of their smallest industrial compressor, the ESH-1 is driven by a 10hp electric motor and is commonly used in the petrochemical industry. Select specifications of the ESH-1 are shown in Table 1.

Table 1. Dresser-Rand ESH-1 specifications

Model:	ESH-1	Max. Temp (°F):	320
Stages:	single	Flow Capacity (ACFM):	34
Piston Diameter:	6"	Compressor (BHP):	7
Stroke:	5"	Weight (lbs):	∼8,000
Max. Pressure (psia):	50	Speed (RPM):	360

The ESH-1 is an intermittent flow, positive displacement air compressor with a single piston which pressurizes cylinders on both sides of the piston head, denoted as crank-side cylinder and head-side cylinder. The compressor can be operated under full load (both cylinders being compressed), half-load (only one cylinder compressed), or no load. Each cylinder has a set of inlet suction valves which allow air to be drawn in at atmospheric pressure, and a set of discharge valves which allow compressed air to be discharged into a discharge tank. The valve assembly, shown in Fig. 3, includes 16 individual valves, each with a poppet valve and spring to keep valves closed until a pressure imbalance is achieved.

The ESH-1 compressor test cell is outfitted with a comprehensive data acquisition system to capture measurements during compressor operation. The specific sensors utilized for this work are an accelerometer (Triaxial PCB 356A16) mounted on the crank-side discharge valve manifold (Fig. 4), an angular encoder (Photocraft HS20.5QZ) mounted on the main crank shaft, and two in-cylinder pressure transducers (Omega PX309-100AI) to measure both cylinder pressures. Sensor measurements are collected at 20 kHz by a National Instruments CompactDAQ system with 9213, 9234, 9401, and 9203 DAQ modules with an interface developed in LabView to view sensor readings and export data for post processing.

4. FAULT SEEDING & METHODOLOGY

While compressor valves experience several different fault conditions, the one chosen for this study is valve seat wear because of its likelihood of occurrence from field data. The valve seat as identified in Fig. 3 can experience a gradual loss of thickness due to poppet impact and torsional rubbing from the helical spring. This slowly increases the distance which

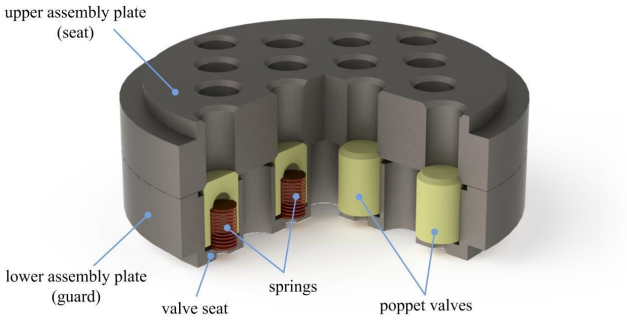

Figure 3. Poppet Valve Assembly

the valve poppet travels during opening and closing, increasing gas flow and valve impact force. To avoid introducing permanent valve seat damage by purposefully removing seat material, the effect was recreated by removing a precise amount of material from the bottom of the valve poppet. The degree of valve seat wear is delineated as 0" removed (nominal) from poppet, 1/32" removed, and 1/16" removed. These poppet conditions are illustrated in Fig. 5.

Table 2. Valve seat wear cases

Fault Case	Group 1	Group 2	Group 3	Group 4
Case 1	0"	0"	0"	0"
Case 2	0"	1/32"	1/32"	0"
Case 3	1/32"	1/32"	1/32"	1/32"
Case 4	1/32"	1/16"	1/16"	1/32"
Case 5	1/16"	1/16"	1/16"	1/16"

It is assumed that the sixteen valves in the valve assembly (shown in Fig. 3) degrade gradually and non-uniformly, generating mixed degrees of conditions within the assembly. To accomplish this, the valves are divided into four valve groups as shown in Fig. 5 - [top] with valves in each group seeded with the same fatigue severity. Five valve seat wear cases are seeded by assigning all poppets in a valve group to one of the three states of wear. The cases investigated are shown in Table 2. Each fault condition investigated is introduced to only the crank-side discharge valves while the head-side discharge valves and all suction valves remained in their original, healthy state as provided by the manufacture. To maintain consistency during data collection, the compressor is operated at full load with constant discharge tank pressure.

Compressor vibration is measured while operating with healthy valves and with increasing degrees of degradation through deliberate fault seeding. For each fault case investigated, raw vibration data is decomposed into individual machine cycles using the crank shaft position measurement. A time-frequency analysis is then performed, resulting in multiple TFD's for each case. A region-of-interest, representing a zoomed region of the entire time-frequency spectrum, is identified on the TFD's which exhibited observable energy change between fatigue cases during the time of discharge valve activity. The region-of-interest is isolated and processed as an image by extracted property features from the gray-scale. A feature vector of image statistics is created for each isolated region-of-interest and represents a single observation. All observations for a particular fault case are separated into a classifier training set and a validation set. The training set is used to train a linear and quadratic classifier. The validation feature set is then used to assess the performance of the classifiers to correctly identify the actual fault case. An overview of the proposed detection and classification methodology is shown in Fig. 6.

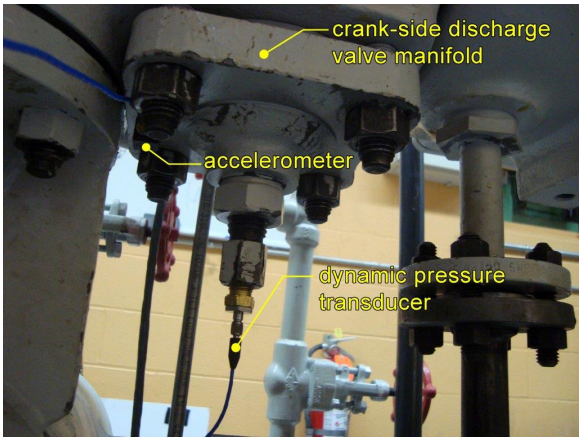

Figure 4. Crank-side discharge valve manifold and triaxial accelerometer (PCB 356A16)

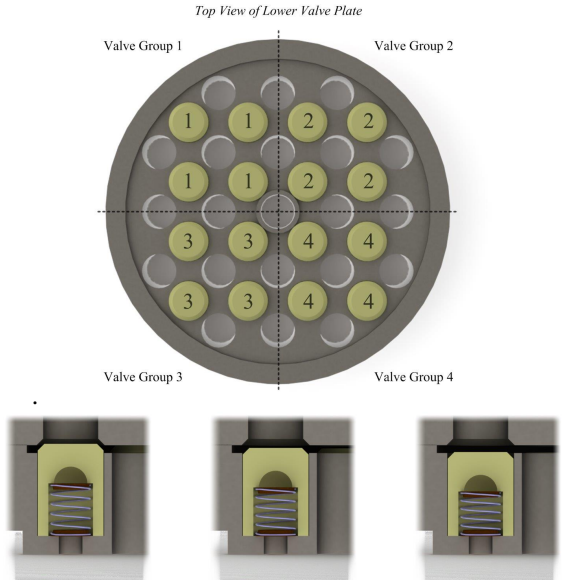

Figure 5. [top] - Valve Groupings, [bottom] - Nominal, Degraded 1 (-1/32"), Degraded 2 (-1/16")

4.1. Signal Processing

Post data-collection signal processing involves decomposing the raw vibration signals into individual machine cycles and performing time-frequency analysis. Figure 7 shows a one second sample of raw vibration data collected during compressor operation. Also shown is the crank and head-side cylinder pressures during that time frame.

As expected, the highest intensity vibrations occurs during the opening and closing of the crank and head-side discharge valves as each cylinder reaches discharge pressure. Less intense vibration, in between discharge valve activity, is related to the opening and closing of the inlet suction valves. In

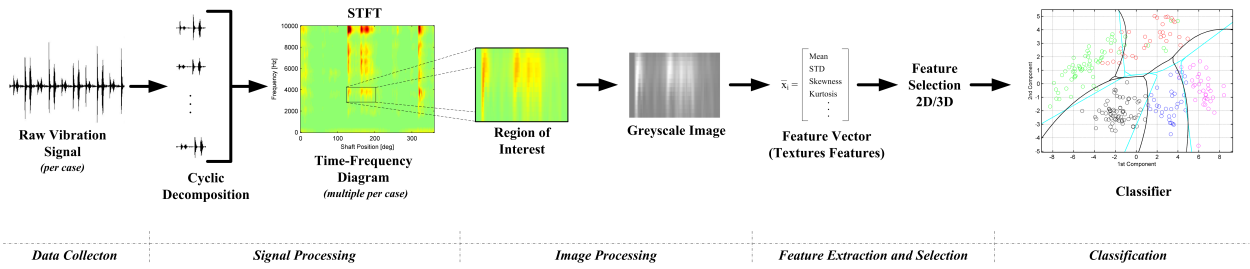

Figure 6. Methodology overview

preparation for time-frequency analysis, each data set collected is decomposed into individual machine cycles using crank shaft position measurement to establish the beginning and end of a crank cycle. An STFT is generated for each cycle and then averaged over ten cycles to generate a single TFD, or observation. A five cycle overlap is used to increase the number of observations per data set and promote TFD consistency. The result is multiple TFD's per data set representing experimental observations from the particular fault case.

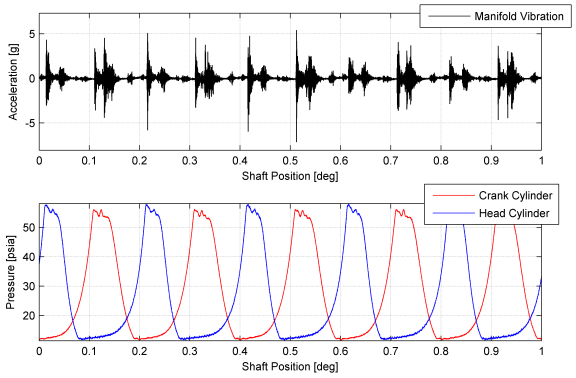

Figure 7. Raw vibration signal (top) and cylinder pressure (bottom) 100% load

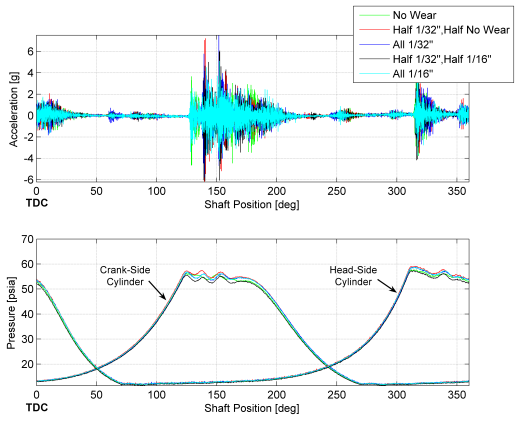

Figure 8. Cyclic decomposition of vibration and pressure signals for each fault condition and case

4.1.1. Cyclic Decomposition and Conversion to Angular Domain

The numbers of data samples per cycle, N_{cycle}, is determined via the crank shaft position as provided by the rotary encoder sensor. The operating rpm of the ESH-1 is essentially constant with negligible variation. Under these conditions the crank shaft position is a linear function of time and therefore sample rate. Thus the degrees per sample is $\Theta_{sample}\frac{360^\circ}{N_{cycle}}$. The number of samples per cycle varied slightly between data sets but was found on average to be 4012 samples/cycle with an average Θ_{sample} of 0.0897 degs/sample. Based the Θ_{sample} calculated for each data set, vibration and pressure data is converted to the angular domain and separated into sets of 360° cycles. The total number of cycles extracted for each fault case varied based on the amount of data available. Figure 8 shows the raw vibration and cylinder pressures for a single machine cycle.

Its apparent from Fig. 8 that each fault case has a relatively unique vibration pattern. Analysis is focused on vibrations during operation of the crank-side discharge valves, therefore a shaft position of 0° is set to correspond with a piston position of top-dead center. This positions the opening of crank-side discharge valves near mid cycle or bottom dead center between shaft positions of 120° and 220°.

4.1.2. Time-Frequency Analysis

As seen in Fig. 8, the vibration signal for a complete machine cycle is non-stationary and appears to be a function of shaft position. Time-frequency diagrams created via the short-time Fourier Transform are used to investigate the frequency content as a function of shaft position. Using Eqn (1), the STFT representing the raw vibration signal is found for each decomposed cycle using a 50 sample window length, 75% window overlap, and a half sine window shape. To reduce noise and better reveal stationary periodic behavior, the STFT is averaged over 10 machine cycles as shown in Eqn. (2)

$$STFT_{avg}(\tau,k) = \frac{1}{M}\sum_{n=1}^{M} STFT_n(\tau,k) \qquad (2)$$

where $M = 10$ and τ is now a shaft-position window segment in the angular domain and not the time domain. A single cyclic averaged STFT for each case calculated with one condition (Case 5) shown in Fig. 9.

The time-frequency diagrams show distinct frequency activity occurring from 120° to 220° and from 320° to 20°. These shaft positions coincide with discharge valve activity from the crank-side and head-side respectively. The STFT parameters (window size, shape, overlap, etc) used provide reasonable angular resolution but with some frequency smearing.

4.1.3. Identifying Region-of-Interest

The STFT shows a wide range of frequency content in the raw vibration signal during the time of valve operation. However, it is determined to target frequency regions within each fatigue case which showed cross-case variation with inner-case consistency. Through careful observation of the TFD in areas within the discharge valve operation window and through an ad hoc modal analysis when the compressor is off, a region-of-interest (ROI) is identified. The nature of the poppet impact with the valve seat is a form of impulse input and as such one would expect compressor structural natural frequencies to be present in the measurement.

The frequency range selected is 3 kHz to 4.2 kHz between a shaft position of 120° to 220° as shown in the boxed region in Fig. 9. This region shows noticeable shape and intensity variation between fault condition cases predominately in the 3.8 kHz area. This frequency is shown for Case 5 in Fig. 9 and likely represents a natural frequency of the compressor excited by valve dynamics. This ROI is then extracted from every STFT observation from all cases reducing the image size drastically while still focusing on the key valve opening

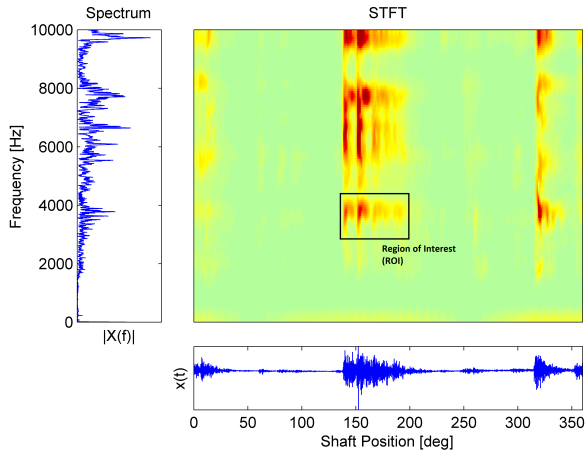

Figure 9. Case 5: all 1/16"wear : A singular **STFT** observation ($M = 10$, 50 sample window length, 75% overlap, half-sine window, linear scale). Region of Interest (ROI) [box]

event. These ROI's are then used to determine a feature vector for each observation.

4.2. Feature Extraction

Feature extraction is a data reduction technique in which a sub-set of properties, or *features*, are used to represent a larger data object, such as an image. These *features* are compiled into a *feature vector*, $\bar{x}$, which contains k calculated *features* x_i, where $i = 1, 2, ..., k$ for a given observation as shown in Eqn. (3).

$$\bar{x} = [x_1,\ x_2,\ x_3,\ \ldots\ ,\ x_k]^T \tag{3}$$

Feature extraction is generally the first step in pattern recognition problems which seek to identify, or classify, objects using features which best describe the original object, or class of object. In this work, the ROI from each TFD is isolated and image-based statistical features are extracted by processing each ROI as an image. The features chosen to characterize each image include texture properties that quantify intensity gradients when the image is converted into a gray-scale representation. A feature vector is extracted for every observation and organized by TFD and fatigue case. The isolated ROI from a sample TFD and fatigue case observation is shown in Fig. 10 (see the bottom image for the $1/16''$ wear case).

The texture of an image can be described as smooth, rough, bumpy, etc. Analysis of the spatial relationships and intensity gradients allow for quantification of such textural descriptions. The texture features extracted are divided into two groups, 1^{st} order statistics and 2^{nd} order statistics. The gray-scale representation of the ROI has a range in intensity from 0 (representing black) to 1 (representing white) at discrete levels. Each TFD is treated as an $M \times N$ image with each element value representing a pixel intensity value $I(m, n)$. To reduce the value range of $I(m, n)$ and localize intensity gradients around areas which showed the greatest distinction among fault cases (and attenuate higher magnitudes which may have skewed the analysis), intensity values are mapped to a new min and max according to Eqn. (4).

$$I(m,n) = \begin{cases} I_{min}, & if\ I(m,n) \leq I_{min} \\ I(m,n), & if\ I_{min} < I(m,n) < I_{max} \\ I_{max}, & if\ I(m,n) \geq I_{max} \end{cases} \tag{4}$$

The amplitude spectrum within the ROI vary from approximately -10 to 40. Various values of I_{max} and I_{min} are tested and evaluated based on visual distinction of the region and how well object boundaries are identified. Mapping values of 8 and -8 were chosen which appeared to maximize gradients and object delineation within the region of 3.8 kHz. These values are maintained for every ROI to ensure visual consistency between cases and faults. $I(m, n)$ is then normalized to have a value range of 0 to 1, and binned into N_{gray} discrete intensity values to facilitate texture feature calculations. Ex-

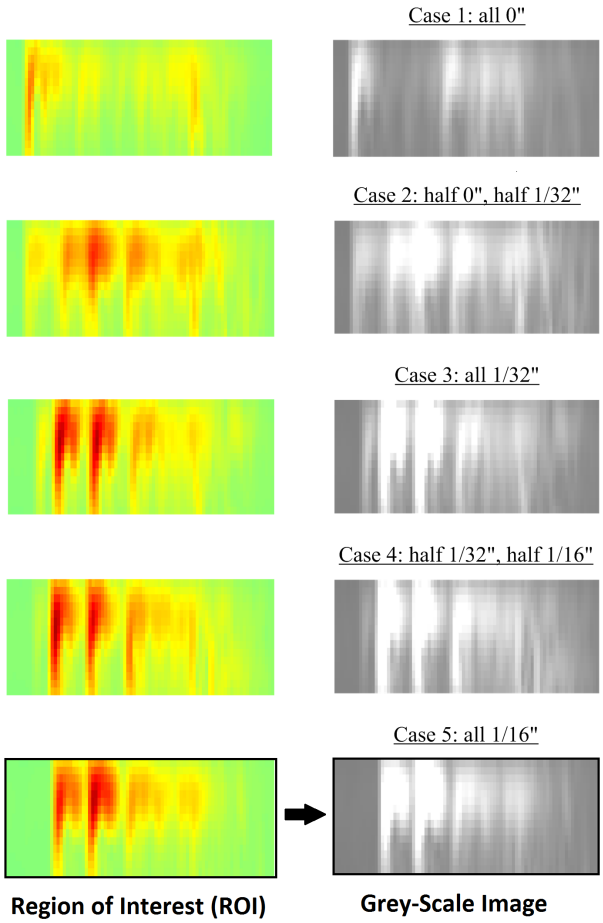

Figure 10. Valve Seat Wear ROI images extracted from a sample TFD for each case: STFT (*left*), Grey-scale (*right*)

amples of ROI gray-scale representations using $N_{gray} = 256$ is seen in Fig. 10.

Next, 1^{st} and 2^{nd} order statistics are calculated and result in 13 metrics representing each observation. First order statistics provide information about the overall gray level distribution of the image as a whole (Theodoridis & Koutroumbas, 2008). These include the following five metrics: mean, standard deviation , skewness, and kurtosis which are the average, dispersion, asymmetry, and peakedness about mean intensity, respectively; and entropy which is the measure of histogram uniformity. Table 3 outlines the image statistic along with the corresponding equation.

Second order statistics provide additional information about the relative location of gray levels. To extract these features, a gray-level co-occurrence matrix (GLCM) is created from the gray-scale intensity image (also described as a Gray-tone Spatial-Dependence Matrix by Haralick (Robert M. Haralick, 1973)). The GLCM contains information which characterizes the texture of an image and the features extracted help describe the spatial relationship, transitional intensity, and general complexity of gray levels within the image.

The GLCM describes how often a pixel of gray value i is neighbored by a pixel of gray level j within a specified direction (in degs) and distance (in number of pixels), collectively described as the offset. When analyzing a gray-scale image with N_{gray} discrete intensity levels, the resulting GLCM is a $N_{gray} \times N_{gray}$ square matrix with element values $p(i,j)$ equaling the number of occurrences for a particular pixel intensity pair (i,j) at the specified offset. The matrix $p(i,j)$ is thus given by

$$\begin{aligned} & p(i,j)_{\delta_m,\delta_n} = \\ = & \sum_{m=1}^{M}\sum_{n=1}^{N}\begin{cases} 1, & if\ I(m,n)=i \\ & and\ I(m+\delta_m, n+\delta_n)=j \\ 0, & otherwise \end{cases} \end{aligned} \quad (5)$$

where i and j are image intensity values, m and n are pixel position coordinates in the image $I(m,n)$, and (δ_m, δ_n) represent the offset based on the selected direction and distance. The resulting matrix can also be viewed as a second order histogram in which gray levels are considered in pairs with a specified spatial relationship, unlike a first order histogram where only single gray levels are considered.

The second order statistics shown in Table 3 are calculated for the resulting GLCM matrices. From each statistic, the mean and range value across all GLCM matrices are used as features, resulting in eight total features per ROI.

4.3. Feature Selection

All ROI observations, represented by feature vectors, are divided into five groups by fatigue level. There are 13 total features extracted from each observation and the total number of observations for each case are: 244 - Case #1, 271 - Case #2, 135 - Case #3, 135 - Case #4, and 271 - Case #5. The irregular number of observations is due to the amount of data collected resulting in varying number of compressor cycles. Recall, that each observation is the result of the average STFT of 10 cycles so this still is a relatively large sample size.

All feature vectors are combined into a $13 \times N_i$ case array, where N_i is the number of observations within that fatigue case and each row is one of 13 features. From the total observations in each case, 75% are randomly selected for classifier training and the remaining 25% used for validation of the classification model.

There are many well documented methods of feature selection. Some utilize the ability for a given feature to discriminate between classes as in a standard $t-test$, others require the classifier to be part of the selection. For this exploratory work an exhaustive search method is applied. The dimension of the classifier is chosen to be three or less to allow for visualization. Then every feature variable permutation,

Table 3. 1^{st} and 2^{nd} order statistics for texture-based feature extraction

Statistic	Description	Equation
Mean $(1^{st} moment)$	average intensity of image	$\mu = E\left[I_{m,n}\right] = (\frac{1}{N})(\frac{1}{M})\sum_{m,n} I(m,n)$
Standard Deviation	dispersion from the mean intensity	$\sigma = \sqrt{E\left[(I(m,n)-\mu\right]^2}$
Skewness $(3^{rd} moment)$	asymmetry about mean intensity	$s = \frac{E\left[(I(m,n)-\mu\right]^3}{\sigma^3}$
Kurtosis $(4^{th} moment)$	degree of peakedness about mean intensity	$k = \frac{E\left[(I(m,n)-\mu\right]^4}{\sigma^4}$
Entropy	measure of histogram uniformity	$e = -\sum_{k=0}^{N_g} P(I_k)\log_2 P(I_k)$
	where $P(I_k)$ =(# of pixels at intensity level I_k) / (total number of pixels in the image).	
Contrast	measure of local gray level variation(A. Gebejes, 2013)	$\sum_{i,j}^{N_g} \lvert i-j\rvert^2 p(i,j)$
Correlation	measure of local gray level linear dependence(Robert M. Haralick, 1973)	$\sum_{i,j}^{N_g} \frac{(i-ui)(j-uj)p(i,j)}{\sigma_i\sigma_j}$
Energy $(angular\ 2^{nd}\ moment)$	measure of uniformity	$\sum_{i,j}^{N_g} p(i,j)^2$
Homogeneity (*inverse difference moment*)	measure of closeness of element distribution to diagonal(A. Gebejes, 2013)	$\sum_{i,j}^{N_g} \frac{p(i,j)}{1+\lvert i-j\rvert}$

up to third dimension, is attempted on the training data and the validation successful classification rate calculated. The group with the highest success represented the set of features with greatest class distinction. While this is more of a "brute force" method it does ensure the optimum classifier is chosen for the desired dimension and given training data at the expense of minor computational effort. Other feature extraction approaches are suggested for future work.

4.4. Classification

The general classification method used for this work is a supervised classifier based on Bayes Decision Theory which requires a set of "training" data with known class membership to infer the most probable class of unknown observations. It is assumed that the training data is normally distributed within each class to simplify the classification model. The classes to which observations are assigned include one of the five fatigue cases. Two types of Bayes classifiers are investigated, a linear discriminant classifier (LDC) and a quadratic discriminant classifier (QDC). Performance of the classifiers are evaluated by comparing the predicted classes of both the training set and a validation set to their known classes. The overall classification accuracy is used to assess how well the proposed methodology and associated time-frequency technique produced unique fault signatures of the valve seat wear cases tested.

5. RESULTS

Applying the described methodology, the valve seat wear fault condition is seeded in the ESH-1 compressor under five possible cases, representing various degrees of severity, and vibration data is collected. Raw vibration data is processed through a transformation from the time to angular position domain. Time-frequency diagrams are determined and image-based features extracted. The resulting features are exhaustively search by training linear and quadratic discriminant classifiers. Each classifier is evaluated on its ability to correctly classify a validation data set with feature space dimensions not exceeding three. Detailed results for four scenarios are given as follows with the features resulting in the highest classification of the validation data using a quadratic classifier depicted.

Figure 11 shows the classification results from a two-dimensional classifier (linear and quadratic) trained with three levels of uniform valve seat wear ($0''$, $1/16''$, $1/32''$). These cases do not consider blended faults but with only two features (mean & standard deviation) yields a 99.4% correct classification. Next, is the full blended fault case with only two dimensions, with Fig. 12 showing the result of 91.4% correct classification.

To improve on these results a third dimension is added that still allows for visual representation. The uniform wear condition is repeated in Fig.13 and results in 100% correct classification this time using mean, skewness, and homogeneity features. Lastly, the blended wear case is applied with three features and shown in Fig.14. By adding a third feature the classification success rises to 98.4%.

Given the seeded fault nature of the work the result is excellent. It is noteworthy that the chosen features depicted are ones with the highest classification rate. All four cases show multiple feature permutations met with success greater than 90%. It is expected that future field trials of the proposed methodology may result in fewer candidate features.

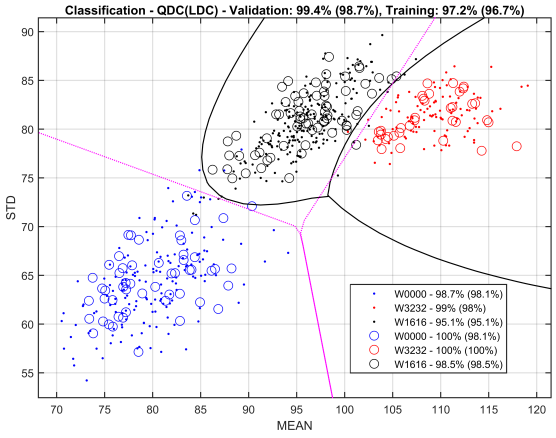

Actual \ Classified	all 0”	all 1/32”	all 1/16”	Totals
all 0”	53 (52)	0 (0)	0 (1)	53
all 1/32”	0 (0)	34 (34)	0 (0)	34
all 1/16”	0 (0)	1 (1)	67 (67)	68
Totals	53 (52)	34 (34)	67 (68)	155

Figure 11. Classification Performance & Confusion Matrix for (**3-class, 2-features**): *Validation* (circles) - QDC: **99.4%**, LDC: **98.7%**, *Training* (dots) - QDC: **97.2%**, LDC: **96.7%**

Actual \ Classified	all 0”	all 1/32”	all 1/16”	Totals
all 0”	53 (52)	0 (0)	0 (1)	53
all 1/32”	0 (0)	34 (34)	0 (0)	34
all 1/16”	0 (0)	0 (2)	68 (66)	68
Totals	53 (52)	34 (36)	68 (67)	155

Figure 13. Classification Performance & Confusion Matrix for (**3-class, 3-features**): *Validation* (circles) - QDC: **100%**, LDC: **98.1%**, *Training* (dots) - QDC: **99.3%**, LDC: **98.9%**

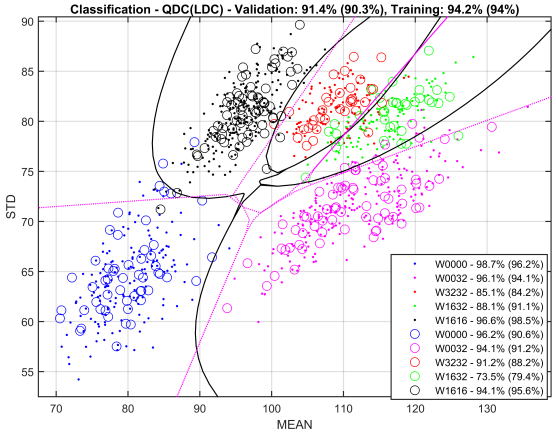

Actual \ Classified	all 0”	0 / 1/32”	all 1/32”	0 / 1/16”	all 1/16”	Totals
all 0”	51 (48)	0 (0)	0 (0)	0 (0)	2 (5)	53
0” / 1/32”	0 (0)	64 (62)	0 (0)	4 (6)	0 (0)	68
all 1/32”	0 (0)	0 (0)	31 (30)	2 (2)	1 (2)	34
0” / 1/16”	0 (0)	2 (1)	7 (6)	25 (27)	0 (0)	34
all 1/16”	1 (1)	0 (0)	3 (2)	0 (0)	64 (65)	68
Totals	52 (49)	66 (63)	41 (38)	31 (35)	66 (72)	257

Figure 12. Classification Performance & Confusion Matrix for (**5-class, 2-features**): *Validation* (circles) - QDC: **91.4%**, LDC: **90.3%**, *Training* (dots) - QDC: **94.2%**, LDC: **94.0%**

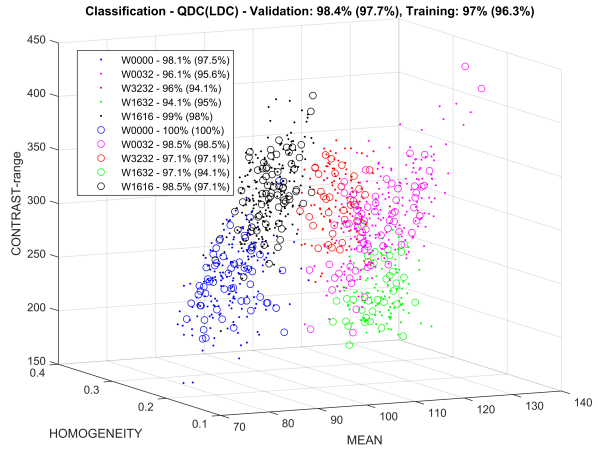

Actual \ Classified	all 0”	0 / 1/32”	all 1/32”	0 / 1/16”	all 1/16”	Totals
all 0”	53 (53)	0 (0)	0 (0)	0 (0)	0 (0)	53
0” / 1/32”	0 (0)	67 (67)	0 (0)	1 (1)	0 (0)	68
all 1/32”	0 (0)	0 (0)	33 (33)	1 (1)	0 (0)	34
0” / 1/16”	0 (0)	0 (1)	1 (1)	33 (32)	0 (0)	34
all 1/16”	0 (0)	0 (0)	1 (2)	0 (0)	67 (66)	68
Totals	53 (53)	67 (68)	35 (36)	35 (34)	67 (66)	257

Figure 14. Classification Performance & Confusion Matrix for (**5-class, 3-features**): *Validation* (circles) - QDC: **98.4%**, LDC: **97.7%**, *Training* (dots) - QDC: **97.0%**, LDC: **96.3%**

6. CONCLUSION

The aim of this work is to develop a vibration-based condition monitoring method for early detection of valve seat wear in reciprocating compressors. Vibration data was processed using time-frequency analysis and image pattern recognition

techniques are used to extract fault identifying features. Results indicate the short-time Fourier transform provides an excellent ability to capture fault signatures which are successfully quantified using image-based statistical features. The method produces features which results in greater than 90% classification rates in just two and three-dimensional feature spaces. The performance achieved is particularly encouraging when considering the mixed fatigue gradients investigated. The process developed produced promising results with room for optimization and investigation to assess limitations and expand capabilities.

Future work is planned by considering other common valve failure modes like poppet spring fatigue. In addition blended fault conditions need to be addressed since it is unlikely that the wear conditions are uniform across the valve. Finally, preliminary work has already begun to utilize more features either through intelligent selection or by feature extraction (PCA).

REFERENCES

A. Gebejes, R. H. (2013). Texture characterization based on grey-level co-occurrence matrix. In editor (Ed.), *Conference of informatics and management sciences.*

Antoni, J. (2009). Cyclostationary by example. *Mechanical Systems and Signal Processing*, *23*, 987-1036.

Elhaj, M., Almrabet, M., Rgeai, M., & Ehtiwesh, I. (2010). A combined practical approach to conditionmonitoring of reciprocating compressors using ias and dynamic pressure. *International Journal of Mechanical, Aerospace, Industrial, Mechatronic and Manufacturing Engineering*, *Vol 4*(No. 3).

Elhaj, M., Gu, F., Ball, A., Shi, Z., & Wright, J. (2001). Early detection of leakage in reciprocating compressor valves using vibration and acoustic continuous wavelet features. In *Condition monitoring and the diagnostic engineering managemen: Comadem 2001t* (p. 179-756).

Guerra, C. J., & Kolodziej, J. R. (2014). A data-driven approach for condition monitoring of reciprocating compressor valves. *ASME Journal of Engineering For Gas Turbines and Power*, *136*(4).

Holzenkamp, M., Kolodziej, J. R., Boedo, S., & Delmotte, S. (2016, June). Seeded fault testing and classification of dynamically loaded floating ring compressor bearings. *ASCE-ASME Journal of Risk and Uncertainty in Engineering Systems Part B: Mechanical Engineering*, *2*.

Liang, B., Gu, F., Ball, A., & Henry, T. (1996). A preliminary investigation of valve fault diagnosis in reciprocating compressors. *Maintenance & Asset Management Journal*, *11*(2), 2-8.

Randall, R. B. (n.d.). *Vibration-based condition monitoring: Industrial, aerospace and automotive applications* (1st ed.). John Wiley.

Robert M. Haralick, I. D., K. Shanmugam. (1973, November). Texture features for image classification. *IEE Transactions on System, Man, and Cybernetics*, *Vol SMC 3*(No.6).

Schirmer, A. G. F., Fernandes, N. F., & Caux, J. E. D. (2004). On-line monitoring of reciprocating compressors. In *Npra maintenance conference.*

Theodoridis, S., & Koutroumbas, K. (2008). *Pattern recognition 4th edition* (4th ed.). Academic Press.

Yih-Hwang, Liu, H.-S., & Wu, C.-Y. (2006). Automated condition classification of a reciprocating compressor using time-frequency analysis and an artificial neural network. *Smart Materials and Structures*, *15*, 1576-1584.

Yih-Hwang, Liu, H.-S., & Wu, C.-Y. (2009). Automated valve condition classification of a reciprocating compressor with seeded faults: experimentation and validation of classification strategy. *Smart Materials and Structures*, *18*, 1-20.

Zouari, R., Antoni, J., Ille, L., Sidhamed, M., Willaert, M., & Watremetz, M. (2007). Cyclostationary modelling of reciprocating comrpessors and application to valve fault detection. *International Journal of Acoustics and Vibration*, *12*(3), 116-124.

BIOGRAPHIES

John N. Trout is currently pursuing a M.Eng. in Mechanical Engineering at the Rochester Institute of Technology in Rochester, NY with expected completion in May 2016. He received a B.S. in Integrated Science and Technology in 2006 from James Madison University located in Harrisonburg, VA. His professional background includes the design and development of distributed generation projects for renewable energy systems. Member ASME.

Jason R. Kolodziej is an Associate Professor of Mechanical Engineering at the Rochester Institute of Technology (RIT) in Rochester, NY. He received his Ph.D. in mechanical engineering from the State University of New York at Buffalo in 2001 with a research focus in controls and nonlinear system identification. For eight years he worked in industry for General Motors Fuel Cell Activities as a Sr. Research Engineer with principle duties in hybrid electric-fuel cell vehicle powertrain controls and system architecture. To date he has been granted 10 U.S. Patents. His present research focus is the study of fault detection, diagnosis, and prognostic health assessment of engineering systems. He currently has funded projects covering a wide range of industrial applications from: electromechanical actuators in aircrafts to fuel cell automotive powertrains to large scale compression equipment. He is a member of the ASME. In 2012, he was awarded RITs prestigious Eisenhart Provost Award for Excellence in Teaching.